Lowest Triplet State of Indole: An ab Initio Study

David K. Hahn and Patrik R. Callis*

Department of Chemistry and Biochemistry, Montana State University, Bozeman, Bozeman, Montana 59717

Received: October 14, 1996[⊗]

Ab initio electronic structure calculations at the CIS/3-21G and CIS/6-31G(p,d) levels on the ^3L_a state of indole confirm that its permanent dipole is much smaller than that of its singlet counterpart, ^1L_a—despite having nearly the same configuration content—and they predict that it is even smaller than that of the ground state because the electron density shift is opposite that for the ^1L_a transition. This not only explains why the phosphorescence of indole derivatives, including tryptophan, has well-defined vibronic structure in polar media, whereas the fluorescence from ^1L_a is broad and nearly featureless, but also suggests that the tryptophan phosphorescence spectrum maximum for proteins at low temperature may be anticorrelated with the fluorescence maximum. Reasons for the difference are traced to interference terms involving minor configurations that have considerable leverage on the permanent dipole because of large transition dipoles between the minor and major configurations. Fluorescence and phosphorescence vibronic band shapes were calculated using these wave functions and are in good qualitative agreement with experimental results.

Introduction

The fluorescence and phosphorescence from the amino acid tryptophan are used extensively as intrinsic internal probes of protein structure and dynamics.[1−6] The chromophore for the low-lying electronic transitions of interest is the indole ring. Both fluorescence and phosphorescence from most indole compounds are believed to originate from a state designated as L_a, which molecular orbital (MO) methods of many varieties[7−11] describe as being primarily an excitation from the highest occupied canonical Hartree−Fock molecular orbital (HOMO) to the lowest unoccupied MO (LUMO), with a significant admixture of excitation from HOMO − 1 to LUMO + 1. Because this configuration interaction (CI) picture holds for both ^1L_a and ^3L_a, an underlying question for many years has been why the fluorescence (from ^1L_a) of indole compounds shows only slight structure, whereas the phosphorescence under similar conditions invariably has much sharper vibronic structure.

There is now considerable evidence supporting the long-held view that the ^1L_a state has a much greater dipole than does the ground state.[12−14] The blurring of vibronic features in polar media therefore comes from inhomogeneous broadening, the result of each molecule in a solution experiencing a unique local electric field from its environment.[15,16] The large dipole change means that the individual molecular transition energies will be distributed over a wide range. An obvious conclusion, then, is that the ^3L_a state must have a much smaller dipole than the ^1L_a state. Strong theoretical evidence that this is indeed the case was recently reported by Serrano-Andres and Roos[11] as a result of a high-level CASSCF computation, but how the ^1L_a and ^3L_a wave functions differed to cause such a large dipole difference was not discussed.

In this paper we present and analyze ab initio electronic structure calculations at the CIS/3-21 and CIS/6-31(p,d) levels, which also predict that the ^3L_a state has a small dipole—even smaller than that of the ground state—and that the reason lies in surprisingly small differences in the contributions of certain singly excited configurations due to fundamental differences in electron repulsion interaction for singlet and triplet configurations. In addition, geometry differences and vibrational modes are computed and used to compute the emission spectral vibronic band shapes. We find that these wave functions accurately account for the details of the observed phosphorescence spectrum and that they are consistent with the slightly structured ^1L_a fluorescence seen from proteins such as ribonuclease T1.

Methods

All ab initio calculations were performed using the Gaussian 94 program package[17] on an SGI R4400 workstation. CIS/3-21G and CIS/6-31(p,d) single-point calculations were performed on indole at their respective optimized ^1L_a geometry to obtain CIS coefficients for the ^1L_a and ^3L_a electronic states. All the valence and core electrons were included in each CIS calculation. As a test of the effects of geometry on our results, the CIS/3-21G single-point calculations were repeated at the ^1L_b CIS/3-21G optimized geometry of indole, with the Root = 2 option used in the ^1L_a case. The ^1L_a and ^1L_b states were sufficiently separated in energy at the geometries used so that their properties were insensitive to small changes in geometry. We did not use the ground-state geometry because the ^1L_b and ^1L_a states were nearly degenerate and mixed. At all geometries used, the ^3L_a state lies too far in energy below the ^3L_b state for any significant mixing to occur.

A Fortran program was written that, using the CI coefficients from the CIS single-point calculations, converts the dipole moment matrix elements from the atomic orbital (AO) basis to the CI basis. In terms of the MO density matrices, $\boldsymbol{\rho}^{kk}$, and the dipole matrix in the AO basis, $\mathbf{M}^n$, the diagonal elements ($i = k$ and $j = l$) for the nth component of the dipole operator ($n = x, y, z$) are given by

$$M^{n}_{ij,ij} = (\sum 2\boldsymbol{\rho}^{kk} - \boldsymbol{\rho}^{ii} + \boldsymbol{\rho}^{ij}):\mathbf{M}^n \qquad (1)$$

with $\boldsymbol{\rho}^{kk} = \mathbf{c}_k\mathbf{c}_k^{\dagger}$ being the matrix formed by the outer product between the AO coefficient column vector $\mathbf{c}_k$ of the kth MO and its row vector $\mathbf{c}_k^{\dagger}$ and the sum being taken over the MOs occupied in the ground state. The symbol ":" denotes that the double dot product between $\boldsymbol{\rho}^{kk}$ and $\mathbf{M}^n$ (the sum of the products between corresponding matrix elements) is being taken.[18] The nonzero elements of the dipole operator between different configurations ($i = k$ or $j = l$) are given by

[⊗] Abstract published in *Advance ACS Abstracts,* March 1, 1997.

S1089-5639(96)03146-5 CCC: $14.00

$$\mathbf{M}^n_{ij,kl} = (\boldsymbol{\rho}^{ij}\boldsymbol{\delta}_{kl} - \boldsymbol{\rho}^{kl}\boldsymbol{\delta}_{ij}):\mathbf{M}^n \quad (2)$$

Because we used the Hartree−Fock canonical MOs, eqs 1 and 2 give the one-particle density matrix (1PDM) result for the dipole moment matrix elements. The 1PDM has been shown repeatedly to give less accurate results than the CIS density matrix because the latter includes the effect of orbital relaxation caused by the electron rearrangement.[19] For molecules the size of indole, however, the difference is not large. Projection electron density maps and difference maps[20] were generated by Simpson's rule integration of a density grid in the direction perpendicular to the molecular plane out to 4 Å above the plane. The grid had points every 0.1 Å perpendicular to the plane and every 0.1 Å parallel to the plane.

Computed spectra were generated using a procedure found to be effective for predicting the ^1L_b jet-cooled fluorescence.[21] Geometry differences between the ground and excited state used the optimized HF/3-21G geometry for the ground state and the optimized CIS/3-21G geometry for the excited state. The normal modes and frequencies used were from an MP2/6-31G-(p,d) calculation for the ground state. Franck−Condon factors were generated from a Fortran program written by J. Vivian based on the Doktorov[22] algorithm, which makes no approximations beyond assuming harmonic normal modes. In the calculations presented here, however, it was assumed that the excited-state modes were the same as the ground-state modes.

Results

Triplet vs Singlet Dipole. The orientation and magnitude of the permanent dipole for the ^1L_a and ^3L_a states of indole at the CIS/6-31G(p,d) level are shown in Figure 1. Table 1 compares the dipole moments of the ground, ^1L_b, ^1L_a, and ^3L_a states of indole calculated using different basis sets, geometries, and density matrices. It is seen that the ^1L_a state has a much greater dipole moment than the ^3L_a state, regardless of which basis set or density is used. Geometry effects appear to play only a small role in creating this large disparity.

Figure 2 compares contour diagrams of the projection density differences taken from the ab initio results at the 6-31G(p,d) level for ^1L_a and ^3L_a transitions. Pronounced differences can be seen between the two maps, with the most obvious being that the singlet transition causes a large loss of density at N1 whereas the triplet transition causes a large increase in density on C2. This along with more subtle differences leads to a net shift of the electron density in the opposite direction from that for the singlet transition. In the ground state, the dipole points roughly from the center of the benzene ring toward the N, with the positive end toward the N. Thus, ^1L_a excitation adds to the existing dipole to create a larger dipole, whereas ^3L_a excitation cancels the existing dipole, leaving a smaller dipole.

This rather dramatic difference in the electron-transfer direction for the two transitions is surprising, given the superficial similarity of the CIS wave functions of the two states. Table 2 analyzes the source of the dipole difference between ^1L_a and ^3L_a states at the CIS wave function level by tabulating the major contributions from configuration pairs in the expansion of the *x* and *y* dipole expectation value expressions for the respective states. The CIS wave function is a linear combination of spin-adapted Slater determinants (configurations), $|i \rightarrow j\rangle$, which we write as

$$\Psi = \sum a_{ij}|i \rightarrow j\rangle$$

where a_{ij} is the normalized amplitude of the excited configuration for which an electron in MO *i* is replaced by an electron in virtual MO *j*. The expectation value of the *x* component of the dipole operator for a CIS state is therefore the sum:

$$\mathbf{M}^x = \sum_{ij}\sum_{kl}\mathbf{M}^x_{ij,kl} = \sum_{ij}\sum_{kl}a_{ij}a_{kl}\langle i \rightarrow j|\hat{m}_x|k \rightarrow l\rangle \quad (3)$$

The *x* component is the source of most of the disparity between the two states, with $\mathbf{M}^x$ = 3.22 D for ^1L_a and 1.13 D for ^3L_a. Table 2 lists the most significant *ij*,*kl* terms and shows how the disparity arises from the cross terms, which cause considerable cancellation in the case of the triplet.

As Table 2 shows, the largest contributions for both the ^1L_a and the ^3L_a states are $\mathbf{M}^x_{31,32}$ and $\mathbf{M}^x_{30,33}$, which come from the

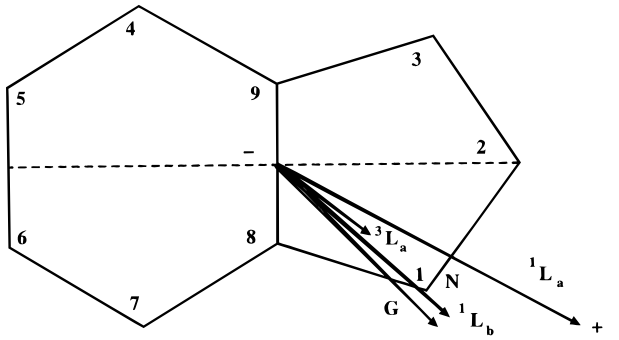

Figure 1. Permanent electric dipoles for the ground, ^1L_a, ^3L_a, and ^1L_b states of indole showing the angle convention used in Table 1 and the ring numbering. The direction angle is measured counterclockwise from the dashed line bisecting the long axis. The dipoles were calculated using the 6-31G(p,d) basis.

TABLE 1: Ground- and Excited-State Dipole Moments

state	method/basis//density	μ^a	θ^b
$^1S_0$	HF/3-21G//SCF	2.02	−45.3
	HF/4-31G//SCF	1.90	−45.6
	HF/4-31G(p,d)//SCF	2.03	−45.1
	HF/6-31G(p,d)//SCF	2.05	−45.3
	HF/6-31++G(p,d)//SCF	2.08	−46.2
	MP2/6−31G(p,d)//MP2	2.19	−47.3
	CASSCF/4s3p1d/2s	1.86[c]	−50[c]
	exptl	2.13[d]	
^3L_a	CIS/3-21G//1PDM	1.53	−34.4
	CIS/3-21G//CIS	1.29	−37.2
	CIS/3-21G//1PDM[e]	1.58	−35.6
	CIS/3-21G//CIS[e]	1.34	−39.9
	CIS/3-21G//1PDM[f]	1.79	−39.0
	CIS/3-21G//CIS[f]	1.61	−41.8
	CIS/4-31G//CIS	1.12	−36.5
	CIS/4-31G(p,d)//CIS	1.39	−36.9
	CIS/6-31G(p,d)//CIS	1.41	−37.3
	CIS/6-31G(p,d)//1PDM[g]	1.68	−34.7
	CIS/6-31G(p,d)//CIS[g]	1.44	−38.5
	CASSCF/4s3p1d/2s	1.47[c]	−34[c]
^1L_a	CIS/3-21G//1PDM	3.42	−20.7
	CIS/3-21G//CIS	3.22	−27.3
	CIS/3-21G//1PDM[f]	3.24	−26.1
	CIS/3-21G//CIS[f]	3.02	−29.7
	CIS/4-31G//CIS	3.03	−27.7
	CIS/4-31G(p,d)//CIS	3.16	−27.9
	CIS/6-31G(p,d)//1PDM	3.38	−21.6
	CIS/6-31G(p,d)//CIS	3.19	−27.9
	CASSCF/4s3p1d/2s	5.69[c]	−12[c]
	exptl	5.4[h]	
^1L_b	CIS/3-21G//1PDM	2.42	−44.0
	CIS/3-21G//CIS	2.15	−41.3
	CIS/4-31G//CIS	2.08	−41.4
	CIS/6-31G//CIS	2.11	−41.2
	CASSCF/4s3p1d/2s	0.85[c]	−41[c]
	exptl	2.3[i]	

[a] Dipole moment magnitude in Debyes at the optimized geometry unless noted. [b] Dipole moment direction in degrees (see Figure 1). [c] Reference 11 at ground-state geometry. [d] Reference 33 . [e] Calculated at CIS/3-21G optimized ^1L_a geometry. [f] Calculated at CIS/3-21G optimized ^1L_b geometry. [g] Calculated at CIS/6-31G(p,d) optimized ^1L_a geometry. [h] Reference 13. [i] Reference 26.

TABLE 2: ^3L_a and ^1L_a CI Dipole Moment Matrix Elements[a] (in Debye)

					^3L_a			^1L_a		
i	*j*	*k*	*l*	$\langle ij\|\hat{m}_x\|kl\rangle$	*a*(*i*,*j*)	*a*(*k*,*l*)	$\mathbf{M}^x_{ij,kl}$[b]	*a*(*i*,*j*)	*a*(*k*,*l*)	$\mathbf{M}^x_{ij,kl}$[b]
					Diagonal Elements					
31	32	31	32	3.446	0.889	0.889	2.721	0.912	0.912	2.866
30	33	30	33	3.508	0.243	0.243	0.208	0.346	0.346	0.421
29	35	29	35	−1.383	−0.266	−0.266	−0.098	−0.107	−0.107	−0.016
29	32	29	32	4.426	−0.117	−0.117	0.061	−0.015	−0.015	0.001
31	33	31	33	7.011	0.052	0.052	0.019	−0.006	−0.006	0.000
28	42	28	42	0.950	0.135	0.135	0.017	0.075	0.075	0.005
31	35	31	35	−2.363	−0.077	−0.077	−0.014	0.014	0.014	0.000
28	33	28	33	2.274	0.078	0.078	0.014	0.004	0.004	0.000
28	32	28	32	−1.291	−0.022	−0.022	−0.001	0.010	0.010	0.000
30	42	30	42	2.184	−0.001	−0.001	0.000	−0.032	−0.032	0.002
					Off-Diagonal Elements					
31	32	29	32	5.990	0.889	−0.117	−1.247	0.912	−0.015	−0.160
31	35	31	32	5.838	−0.077	0.889	−0.796	0.014	0.912	0.150
29	35	29	32	5.838	−0.266	−0.117	0.364	−0.107	−0.015	0.018
31	35	29	35	5.990	−0.077	−0.266	0.244	0.014	−0.107	−0.018
30	33	28	33	−5.393	0.243	0.078	−0.205	0.346	0.004	−0.015
31	33	31	32	−1.069	0.052	0.889	−0.100	−0.006	0.912	0.012
28	42	28	33	4.602	0.135	0.078	0.097	0.075	0.004	0.003
31	32	28	32	−2.127	0.889	−0.022	0.083	0.912	0.010	−0.041
30	42	30	33	4.602	−0.001	0.243	−0.002	−0.032	0.346	−0.103

					^3L_a			^1L_a		
i	*j*	*k*	*l*	$\langle ij\|\hat{m}_y\|kl\rangle$	*a*(*i*,*j*)	*a*(*k*,*l*)	$\mathbf{M}^y_{ij,kl}$[b]	*a*(*i*,*j*)	*a*(*k*,*l*)	$\mathbf{M}^y_{ij,kl}$[b]
					Diagonal Elements					
31	32	31	32	−0.836	0.889	0.889	−0.660	0.912	0.912	−0.695
29	35	29	35	−1.909	−0.266	−0.266	−0.135	−0.107	−0.107	−0.022
30	33	30	33	−2.087	0.243	0.243	−0.124	0.346	0.346	−0.250
29	32	29	32	−0.764	−0.117	−0.117	−0.010	−0.015	−0.015	0.000
31	35	31	35	−1.982	−0.077	−0.077	−0.012	0.014	0.014	0.000
28	32	28	32	−1.774	0.022	0.022	−0.001	−0.010	−0.010	0.000
28	33	28	33	−1.929	−0.078	−0.078	−0.012	−0.004	−0.004	0.000
31	42	31	42	1.362	−0.003	−0.003	0.000	−0.019	−0.019	0.001
					Off-Diagonal Elements					
31	32	29	32	0.796	0.889	−0.117	−0.166	0.912	−0.015	−0.021
31	35	31	32	1.054	−0.077	0.889	−0.144	0.014	0.912	0.027
31	32	28	32	3.252	0.889	0.022	0.127	0.912	−0.010	−0.062
30	33	28	33	−2.592	0.243	−0.078	0.098	0.346	−0.004	0.007
31	33	31	32	1.019	0.052	0.889	0.095	−0.006	0.912	−0.012
31	42	31	32	−3.641	−0.003	0.889	0.019	−0.019	0.912	−0.127

[a] Calculated at CIS/6-31G(p,d) optimized ^1L_a geometry. [b] $\mathbf{M}^n_{ij,kl} = a(i,j) \times a(k,l) \times \langle ij|\hat{m}_n|kl\rangle \times (2 - \delta_{ij,kl})$.

diagonal matrix elements of the HOMO → LUMO and HOMO − 1 → LUMO + 1 transitions, respectively. This is because of the large dipole moments and large CI coefficients (95% of the total ^1L_a wave function) of the $|31 \rightarrow 32\rangle$ and $|30 \rightarrow 33\rangle$ configurations, which are nearly the same for the singlet and triplet. The large dipole difference between the two states stems from what at first seems an insignificant difference in the contribution of minor configurations. The minor configurations contribute significantly when large cross terms exist between the minor configuration and the major one because of a large transition dipole between the two different configurations. Because the dipole operator is a one-electron operator, only those minor configurations that differ from the main configuration by one MO, e.g., $|29 \rightarrow 32\rangle$, $|31 \rightarrow 35\rangle$, etc., can contribute. (The off-diagonal elements in Table 2 have been multiplied by 2 to account for the identical contribution from the transpose matrix element in the symmetric dipole moment matrix.)

It is seen that the minor configuration contributions to the dipole of the ^1L_a state are negligible because their coefficients are so small. In contrast, the triplet state has numerous contributions from minor configurations that are an order of magnitude greater than those for the singlet. The major contributions come from the HOMO → LUMO + 3 ($|31 \rightarrow 35\rangle$) and HOMO − 2 →LUMO ($|29 \rightarrow 32\rangle$) that are large and opposite in sign to the diagonal terms. It is these terms that largely account for the small dipole of the triplet state.

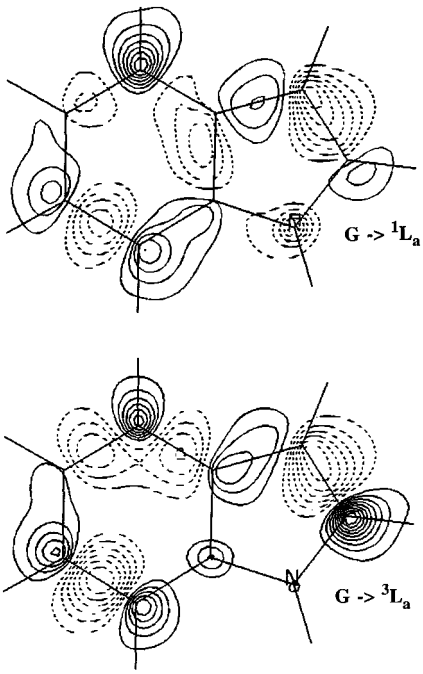

Figure 2. Projection electron density difference contour maps for the ground → ^1L_a and ^3L_a electronic transitions of indole. The projection density is the integral of all electron density above and below a point in the molecular plane. Contours are separated by 0.002 electrons/cubic bohr. Negative electron density changes are given by dashed lines and positive by solid lines.

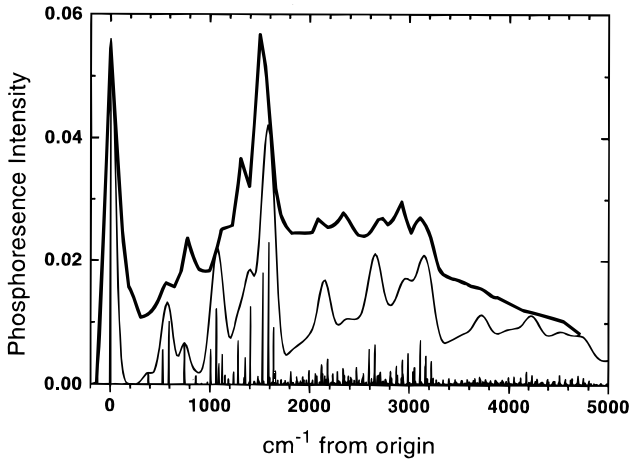

Figure 3. Computed phosphorescence band shapes of indole using line widths of 3 and 120 cm^{-1} (thin lines) compared with the observed phosphorescence from ribonuclease T1 from ref 23 (thick line). The vertical axis provides the Franck−Condon factor for the origin in the computed spectra. The computed spectra are weighted by the emission frequency cubed, with the origin taken as 400 nm. The spectra are plotted relative to their respective origins.

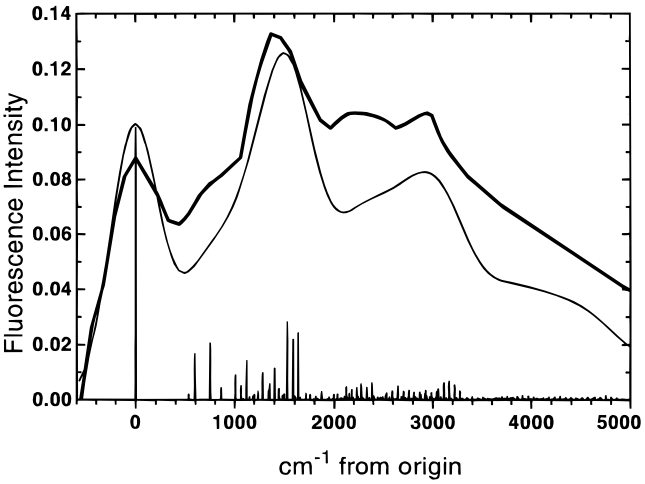

Figure 4. Computed ^1L_a fluorescence band shapes of indole using line widths of 3 and 600 cm^{-1} (thin lines) compared with the observed fluorescence from ribonuclease T1 reproduced from ref 25 (thick line). The vertical axis provides the Franck−Condon factor for the origin in the computed spectra. The computed spectra are weighted by the emission frequency cubed, with the origin taken as 320 nm. The spectra are plotted relative to their respective origins.

The partial list of x components in Table 2 sum to 3.22 D for ^1L_a and 1.37 for ^3L_a, whereas the complete sums are 3.15 and 1.38 D, respectively, so the hundreds of smaller matrix elements not shown here collectively make only small contributions.

Computed Spectra. To help authenticate the wave functions used in the above dipole predictions, we use them to calculate emission spectral band shapes from ^1L_a and ^3L_a. Figure 3 compares the experimental phosphorescence spectrum of ribonuclease T1 at 2 K[23] with that computed using the geometry differences given by CIS/3-21G − HF/3-21G wave functions while using vibrational modes and frequencies from an MP2/6-31G(p,d) treatment of the ground state. The theoretical and experimental spectra are both plotted relative to their respective origins because we are concerned only with the shape of the spectrum. The FC factors, which determine the shape, are mainly determined by the geometry change, which, unlike the energy, is relatively insensitive to dynamic correlation. This procedure reproduces the observed fluorescence shape from the ^1L_b state of indole remarkably well,[21] and it is seen in Figure 3 to match the experimental phosphorescence spectrum quite well also, thereby supporting the accuracy of the wave functions used in this study.

In Figure 4 the ^1L_a fluorescence spectrum, computed in a similar manner, is presented with each line broadened with 3 and with 600 cm^{-1} fwhm Gaussians. Again, the two spectra are relative to their respective origins. The spectrum broadened to 600 cm^{-1} shows vibronic structure in detail similar to that reported for tryptophan in ethanol at 2 K[24] and for ribonuclease T1 at 77K[25], strongly implicating the experimental fluorescence as ^1L_a. The latter experimental spectrum is shown in Figure 4.

Discussion

Triplet Dipole. The excited-state calculations performed in this study are much less sophisticated than the CASSCF procedure used by Serrano-Andres and Roos,[11] which includes all excited configurations, albeit from a restricted "active space" of MOs involving only the π MOs and some diffuse Rydberg orbitals. On top of this is implemented the CASPT2 procedure, a second-order perturbation CI correction to the energy using the CASSCF excited state as reference. This procedure gives vertical excitation energies that are in close agreement between computed and observed transition energies (within about 400 cm^{-1}), and they give 0−0 energies that are within about 1500 cm^{-1} of experimental values. The dipoles and geometries, however, were computed from the CASSCF wave functions, which give vertical transition energies in only moderate agreement with experiment (3700 cm^{-1} too high for ^1L_b and 10 000 cm^{-1} too high for ^1L_a). In the calculations reported here, the ground state is a Hartree−Fock SCF wave function (single closed shell configuration) and the CIS excited states are formed only from singly excited configurations from the ground configuration, although all MOs are involved. As a result, transition energies are far from experimental values on an absolute scale, being 8000−10 000 cm^{-1} too high, depending on basis set quality. From a transition energy point of view, however, the CASSCF procedure is only marginally better than the CIS procedures employed here. This is evident in the computed dipoles, for which the Hartree−Fock SCF and CIS methods give dipoles for the ground and ^1L_b states that are closer to experimental results, although the CASSCF result appears better for the ^1L_a state (Table 1). Relevant here is that no direct measurement of the gas phase ^1L_a dipole has been done; the experimental value comes from fitting solvent shifts to idealized models involving a point dipole in a spherical cavity surrounded by a continuum dielectric.[13] In contrast, the small increase in dipole upon excitation to ^1L_b comes from the measured Stark effect in the gas phase[26] and should be quite accurate. The triplet state dipole is predicted to be smaller than that of the ground state by all the methods listed in Table 1.

In the Results section the reason for the reduced dipole of the ^3L_a state was isolated in terms of certain minor configurations, which were an order of magnitude more important for the triplet than the singlet. One may push the question one step deeper and ask whether the reason for larger contributions of the key configurations is because they lie closer in energy to the HOMO → LUMO configuration in the triplet manifold or because the interactions are stronger. To answer this question, we examined the CI Hamiltonian matrix and found that the interactions were an order of magnitude greater for the triplet, while the energy differences were not substantially different.

The off-diagonal elements of the CI Hamiltonian consist entirely of integrals of the electron repulsion operator. In the present case, only elements between the HOMO → LUMO configuration and those differing by only one MO are relevant. The expression for such an element between configurations $|n$

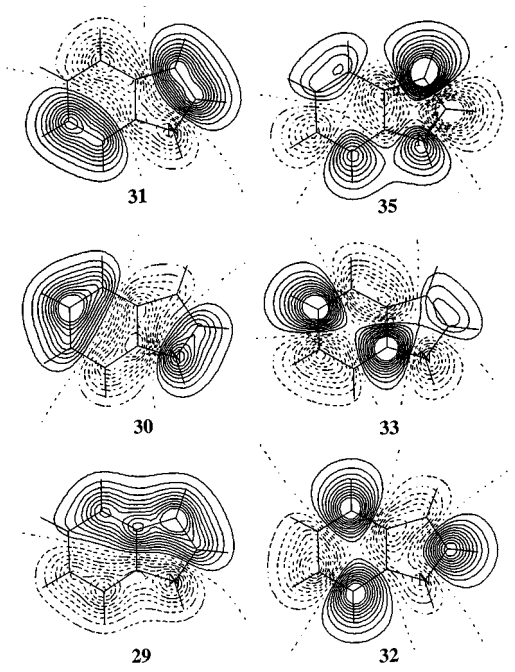

Figure 5. Molecular orbital contour plots for the three highest occupied and three lowest unoccupied π MOs of indole using the 6-31G(p,d) basis. The contours are at 0.7 Å above the molecular plane.

$\rightarrow m\rangle$ and $|n \rightarrow p\rangle$ is given in general terms by[27]

$$\sum[(ii|mp)' - (im|ip)'] \mp (np|nm)'$$

where the notation $(ij|kl)'$ means the repulsion between electron 1 in transition density *ij* and electron 2 in transition density *kl*; the sum is over all occupied MOs, *i*, except *m* and *p*, the prime indicates spin−orbital integration, and the upper sign is for triplets and the lower for singlets.

Thus, the difference in interaction is simply $2(np|nm)$, i.e., twice the repulsion between two one-electron MO products (transition densities) having in common MO *n*. When this integral is large and of opposite sign to the summation in brackets, one can expect to find a larger interaction between the $n \rightarrow p$ configuration and the $n \rightarrow m$ in the triplet compared to the singlet. This happens to be the case for the key configurations noted in the Results section but does not appear to be a general result. The relative size of the important exchange integral, $(np|nm)$, may be estimated by looking at the MOs involved. For such an exchange integral to be large requires that all three MOs (*n*, *m*, and *p*) have large amplitudes on the same atoms. From the MO diagrams in Figure 5 it is seen that MOs 35 and 29 do have large coefficients in common with the HOMO and LUMO (31 and 32). In contrast MOs 33 and 30 have density somewhat complementary to MOs 31, 32, 29, and 35, which results in a small difference in interaction between the singlet and triplet cases.

Because the direction of charge transfer is opposite for the triplet, one is prompted to look for opposite correlation between the experimental fluorescence and phosphorescence shifts in response to environment. This is practical only for nonfluid environments where the emission shift has no contribution due to solvent relaxation after excitation. One example is the single tryptophan emission from the proteins azurin[23] and ribonuclease T1 at low temperature,[23] wherein the fluorescence is at shorter wavelength for azurin and the phosphorescence is at shorter wavelength for ribonuclease T1. In a glycol−water glass at 77 K, however, Purkey and Galley[15] found that red edge excitation caused a red shift of both the fluorescence and phosphorescence of indole.

The latter result does not necessarily mean that there is no dipole reduction in the triplet state. It is well established that differences in dispersion interaction are the source of a universal solvent-induced red shift of absorption and emission spectra of related hydrocarbons such as benzene, naphthalene, and anthracene.[9,28,29] By symmetry these molecules have no dipole and the red shift is in proportion to the polarizability of the solvent. The ^1L_a transition of anthracene, for example, red shifts by over 1200 cm^{-1} when its environment is changed from solid argon to crystalline fluorene.[30] Thus, differences in local polarizability may dominate differences in local electric field when the dipole change is small, as in the case of the indole triplet.

In the case of the red edge effect, the dipole component of the absorption shift is determined by the product of the ground-state dipole and the dipole change. Because the ground-state dipole is small, there is not a large reaction field in the solvent to preferentially stabilize the ^1L_a state. It is possible that enough of the inhomogeneous broadening is due to dispersion forces such that the phosphorescence shows a net red shift as the excitation is scanned to longer wavelengths.

Computed Spectra. The computed stick spectra of Figures 3 and 4 are superficially similar but are quite distinct from similarly computed experimental spectra for the ^1L_b fluorescence.[21] Most notable is that the 0−0 Franck−Condon (FC) factors are 2−4 times lower than for ^1L_b, reflecting the greater geometry changes found for the ^1L_a and ^3L_a states. Whereas for ^1L_b, mode 26 (760 cm^{-1}) is the most FC active, this mode is greatly overshadowed by mode 27 (610 cm^{-1}) and the highest frequency C−C stretching modes, 8 (1616 cm^{-1}), 9 (1576 cm^{-1}), and 10 (1509 cm^{-1}) (frequencies from ref 31). The latter are collectively responsible for the pronounced characteristic maximum near 1550 cm^{-1} in the phosphorescence of indole derivatives. A more detailed discussion is planned in conjunction with higher resolution spectra recently obtained in our laboratory.[32]

Given the large difference in the L_a singlet and triplet dipoles, it is perhaps surprising that the corresponding computed and experimental spectra are so similar. The similarity of the spectra speaks to the similarity of the geometries in the two states. Because the geometry change during an electronic transition is primarily governed by changes in the off-diagonal terms of the density matrix in the AO representation, whereas the dipole change is mainly determined by changes in the diagonal terms, it is quite possible for the two properties to exhibit different changes. The density difference maps (Figure 2) show that the density differences between the two states in the bonding regions are quite similar, despite some pronounced differences near the atoms, suggesting that the vibronic band envelopes for the two transitions should be quite similar. At a detailed level, however, some differences are expected. Overall, there appears to be slightly more pronounced bonding density changes for the triplet transition, and this is reflected in the smaller 0−0 FC factor for the origin (Figures 3 and 4). At a greater level of detail, Figure 2 predicts that the 2−3, 4−9, 4−5, and 6−7 bonds will be larger in the triplet than in the singlet, while the 8−9 bond will be longer for the singlet. These expectations are indeed found in the optimized geometries and lead to differences in the predicted FC factors for the vibrational modes involving major amounts of stretching in these bonds. We are preparing a more detailed analysis for publication.[32]

Conclusions

Ab initio electronic structure calculations at even the modest CIS/3-21G level robustly predict that the lowest triplet of indole (and tryptophan by inference) has a smaller dipole moment than

the ground state. The small predicted difference from the ground state is consistent with the well-known sharp phosphorescence spectra exhibited by these compounds in polar media. Rather small differences between the ^1L_a and ^3L_a wave functions caused by electron repulsion integral differences account for the large dipole of ^1L_a compared to ^3L_a. The calculations also give quite reasonable accounts of the ^1L_a fluorescence and ^3L_a phosphorescence band shapes.

Note Added in Proof. After the manuscript was submitted, it was brought to our attention that a low-temperature correlation of fluorescence and phosphorescence wavelengths for 26 single-tryptophan proteins has been reported (Permyakov, E. A.; Deikus, G. Yu. *Mol. Biol.* **1995**, *29*, 93). In about 10% of pairs of proteins, the fluorescence and phosphorescence wavelengths are anticorrelated.

Acknowledgment. This work was supported by NIH Grant GM31824. We thank Berit Burgess for assistance with some of the figures and Lee Slater for suggesting the use of the projection density.

References and Notes

(1) Demchenko, A. P. *Ultraviolet Spectroscopy of Proteins;* Springer-Verlag: New York, 1986.
(2) Konev, S. V. *Fluorescence and Phosporescence of Proteins and Nucleic Acids*; Plenum: New York, 1967.
(3) Longworth, J. W. In *Excited States of Proteins and Nucleic Acids;* Steiner, R. F., Weinryb, I. Eds.; Plenum: New York, 1971; p 319.
(4) Eftink, M. R. *Methods Biochem. Anal.* **1991,** *35,* 127.
(5) Saviotti, M. L.; Galley, W. C. *Proc. Natl. Acad. Sci. U.S.A.* **1974,** *71,* 4154.
(6) Papp, S.; Vanderkooi, J. M. *Photochem. Photobiol.* **1989,** *49,* 775.
(7) Song, P.; Kurtin, W. E. *J. Am. Chem. Soc.* **1969,** *91,* 4892.
(8) Callis, P. R. *J. Chem. Phys.* **1991,** *95,* 4230.
(9) Chabalowski, C. F.; Garmer, D. R.; Jensen, J. O.; Krauss, M. *J. Phys. Chem.* **1993,** *97,* 4608.
(10) Slater, L. S.; Callis, P. R. *J. Phys. Chem.* **1995,** *99,* 8572.
(11) Serrano-Andres, L.; Roos, B. O. *J. Am. Chem. Soc.* **1996,** *118,* 185.
(12) Andrews, L. J.; Forster, L. S. *Biochemistry* **1972,** *11,* 1875.
(13) Lami, H.; Glasser, N. *J. Chem. Phys.* **1986,** *84,* 597.
(14) Pierce, D. W.; Boxer, S. G. *Biophys. J.* **1995,** *68,* 1583.
(15) Galley, W. C.; Purkey, R. M. *Proc. Natl. Acad. Sci. U.S.A.* **1970,** *67,* 1116.
(16) Demchenko, A. P.; Sytnik, A. I. *J. Phys. Chem.* **1991,** *95,* 10518.
(17) Frisch, M. J.; Trucks, G. W.; Head-Gordon, M.; Gill, P. M. W.; Wong, M. W.; Foresman, J. B.; Johnson, B. G.; Schlegel, H. B.; Robb, M. A.; Replogle, E. S.; Gomperts, R.; Andres, J. L.; Raghavachari, K.; Binkley, J. S.; Gonzalez, C. S.; Martin, R. L.; Fox, D. J.; Defrees, D. J.; Baker, J.; Stewart, J. J. P.; Pople, J. A. *Gaussian 94*; B. Gaussian, Inc.: Pittsburgh, PA, 1996.
(18) Callis, P. R. *Int. J. Quantum. Chem.* **1984,** *S18,* 579.
(19) Foresman, J. B.; Head-Gordon, M.; Pople, J. A.; Frisch, M. J. *J. Phys. Chem.* **1992,** *96,* 135.
(20) Streitwieser, A., Jr.; Collins, J. B.; McKelvey, J. M.; Grier, D.; Sender, J.; Toczko, A. G. *Proc. Natl. Acad. Sci. U.S.A.* **1979,** *76,* 2499.
(21) Callis, P. R.; Vivian, J. T.; Slater, L. S. *Chem. Phys. Lett.* **1995,** *244,* 53.
(22) Doktorov, E. V.; Malkin, I. A.; Man'ko, V. I. *J. Mol. Spectrosc.* **1976,** *64,* 359.
(23) Hershberger, M. V.; Maki, A. H.; Galley, W. C. *Biochemistry* **1980,** *19,* 2204.
(24) Scott, T. W.; Campbell, B. F.; Cone, R. L.; Friedman, J. M. *Chem. Phys.* **1989,** *131,* 63.
(25) Longworth, J. W. *Photochem. Photobiol.* **1968,** *7,* 587.
(26) Chang, C.-T.; Wu, C.-Y.; Muirhead, A. R.; Lombardi, J. R. *Photochem. Photobiol.* **1974,** *19,* 347.
(27) Parr, R. G. *Quantum theory of molecular electronic structure;* W. A. Benjamin, Inc.: New York, 1963.
(28) Shalev, E.; Ben-Horin, N.; Jortner, J. *J. Chem. Phys.* **1992,** *96,* 1848.
(29) Murrell, J. N. *The theory of the electronic spectra of organic molecules*; Wiley: London, 1963; p 94.
(30) Wolf, J.; Hohlneicher, G. *Chem. Phys.* **1994,** *181,* 181.
(31) Takeuchi, H.; Harada, I. *Spectrochim. Acta.* **1986,** *42A,* 1069.
(32) Fender, B. J.; Hahn, D. K.; Callis, P. R. Manuscript in preparation.
(33) McClellan, A. L. *Tables of Experimental Dipole Moments*; Freeman: London, 1963.